2024 IEEE/RSJ International Conference on Intelligent Robots and Systems (IROS)
October 14-18, 2024. Abu Dhabi, UAE

Fractional Order Modeling and Control of Hydrogel-based Soft Pneumatic Bending Actuators

Jesús De La Morena[1], David Redrejo[1], Francisco Ramos[1], Vicente Feliu[1] and Andrés S. Vázquez[1]

***Abstract*— Soft pneumatic bending actuators (SPBAs) are commonly employed in soft robotics due to their unique characteristics, including safety, low weight, speed, and load capacity. However, the combination of pneumatics with soft materials causes SPBAs to exhibit nonlinearities and infinite degrees of freedom, complicating their dynamic modeling. In this work, we present how the dynamics of SPBAs can be adjusted to a fractional order model (FOM), showing an approach for their empirical identification. We also present a method for designing fractional order controllers (FOCs) for this type of actuators, based on the inversion of the empirical FOM. This modeling and control is applied to a modular SPBA made of a smart hydrogel, which endows the actuators with *self-healing*, *self-adhesion*, and *self-sensing* capabilities.**

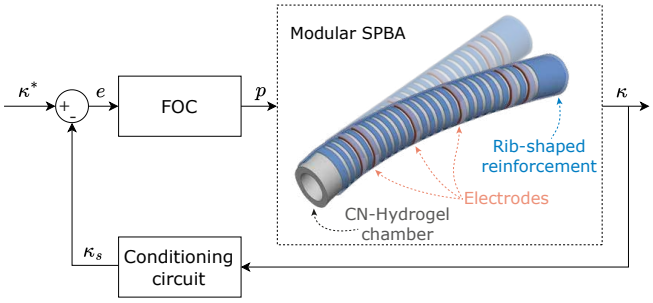

Fig. 1. Concept of a Fractional-Order Control (FOC) scheme for a hydrogel-based Soft Pneumatic Bending Actuator (SPBA).

I. INTRODUCTION

Soft pneumatic bending actuators (SPBAs) are widely used for the actuation of soft robots. The combination of pneumatics with soft materials (e.g., silicone rubbers) offers unique characteristics such as safety, low weight, speed and load capacity, making SPBAs ideal for rehabilitation [1] and delicate manipulation [2]. When smart soft materials (e.g., smart polymers) are used, SPBAs also offer functionalities such as self-healing or self-sensing, which are ideal in pneumatic actuation [3]. However, the use of pneumatics with soft materials comes with the price of nonlinearities and infinite degrees of freedom, which significantly complicates the dynamic modeling and control of soft robots [4].

Several approaches have been taken for modeling SPBAs [5]. Theoretical models are usually based on the use of Newton-Euler or Lagrange formalisms [6]. Analytical models vary in complexity depending on assumptions such as constant or variable curvature, or the existence of hyperelasticity and hysteresis. They range from highly complex, making them difficult to identify and calculate, to highly simplified, which significantly diverge from the actual dynamics of the actuator. Other approaches use finite element method (FEM) models, which are very reliable for quasi-static modeling [7]. Dynamic FEM, while simpler than theoretical modeling [8], also suffers from the material nonlinearities, such as hyperelasticity and hysteresis, requiring sophisticated models that may be challenging to implement and computationally intensive. Lastly, some works propose dynamical models obtained experimentally through the analysis of the responses to step signals at different pressures [9]. However, the models obtained in this way are the simplest and usually neglect important dynamics.

Fractional calculus has been proven as a very powerful tool for adjusting theoretical models to the real dynamics of robotic systems. Although fractional order models (FOMs) have been extensively used for the modeling of rigid and flexible robots [10], there are hardly any studies applied to SPBAs. One of the few related works is the study of Mishra et al., which introduces a fractional-order Bouc-Wen hysteresis model tailored for a pneumatically actuated continuum manipulator [11]. In [12], Huifan et al. propose continuum (but not pneumatic) actuators to be modeled by fractional-order Lagrange dynamics. Both works demonstrate an accurate modeling of the hysteresis of soft actuators but at the expense of complex theoretical development and identification. In this work, we propose a different approach based on the empirical fractional order modeling of SPBAs. Although this modeling is less accurate than analytical FOM, it improves empirical integer-order models (IOM) in terms of precision and simplicity as we demonstrate.

Regardless of the cause of the model inaccuracy, researchers rely on robust and/or adaptive controllers to compensate the behavior of the actuator when it deviates from the modeled dynamics. In this sense, sliding mode controllers are frequently used as they behave well in the presence of nonlinearities [13]. Fractional calculus can also be used for the development of robust controllers. As for modeling, it has been widely used in rigid and flexible robots [14]. Just recently, fractional-order controllers (FOCs) have been studied to control soft robots. A pioneer of these works is [15], where Monje et al. develop two FOCs (a robust FOC and

*This study forms part of the Advanced Materials Programme and is supported by MCIN with funding from European Union NextGenerationEU (PRTR-C17. I 1), by Junta de Comunidades de Castilla–La Mancha (Project SBPLY/21/180501/000135) and by the MCIN/AEI/10.13039/501100011033 FEDER "A way of making Europe" (Grant PID2022-141409OB-C21)

[1] ETS Ingeniería Industrial. Universidad de Castilla-La Mancha, 13071 Ciudad Real, Spain. {jesus.delamorena, david.redrejo, francisco.ramos, vicente.feliu, andress.vazquez}@uclm.es

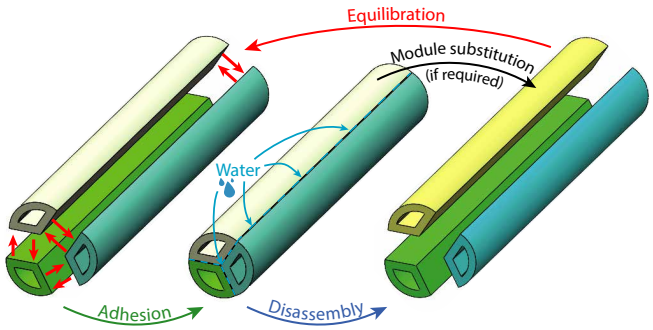

Fig. 2. CN-Hydrogel based modular approach of SPBAs. The modules are joined by contact and can be detached by adding water in the joining interface, allowing the reconfiguration of the actuator.

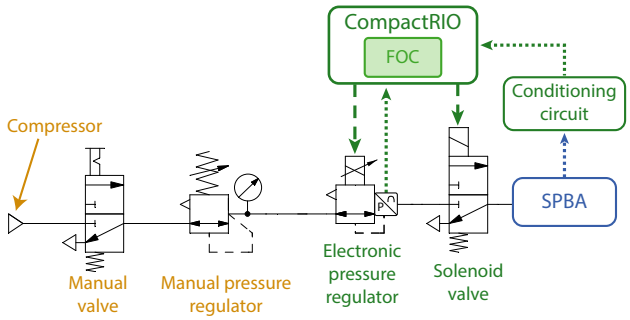

Fig. 3. Pneumatic scheme of the experimental setup used for modeling and control of a unidirectional SPBA. The CompactRIO acquires the SPBA curvature through the conditioning circuit, implements the FOC and commands both the solenoid valve and the electronic pressure regulator while checking the chamber pressure.

an adaptive FOC) to control cable-driven bending actuators. Aligned with the idea of using fractional controllers for overcoming neglected dynamics, in this work we present a fractional control scheme for SPBAs, which is based on a model inversion, possible because of the few parameters involved in our fractional modeling.

II. HYDROGEL-BASED MODULAR SPBA

The modular SPBA used in this work, as presented in [16], is formed of modular air chambers fabricated with our CN-Hydrogel [17] (see Fig. 1). A flexible thermoplastic polyurethane (TPU) rib-shaped reinforcement guides the deformation when the chambers are inflated, allowing the bending actuation and preventing undesired effects such as ballooning. The modular structure, with air chambers of 360°, 180° or 120° cylindrical cross section, allows for the design of different bending actuators: unidirectional (single 360° module), bidirectional (two 180° modules) and tridirectional (three 120° modules).

Moreover, our modular SPBA takes advantage of the *self-x* properties [16] of the CN-Hydrogel:

- The *self-healing* property allows the actuator to self-repair damages (e.g. punctures or overpressure bursts) without external stimuli [17].
- The *self-adhesion* property, based on the same principle as the *self-healing*, allows the material to act as a reversible connection mechanism between modules [18] (see Fig. 2).
- The *self-sensing* property provides the SPBA with proprioception (i.e. curvature sensing) [19]. This *self-sensing* mechanism is similar to that of strain gauges: the elongation of the CN-Hydrogel causes a reduction on its cross section, increasing the electrical resistance.

However, the CN-Hydrogel is hyperelastic and viscoelastic, which, combined with pneumatic actuation, complicates the modeling and control of the SBPA, thus motivating the work presented in the following Sections.

For the sake of simplicity, in this work we present the modeling and control of a unidirectional SPBA. The SPBA is installed in the experimental pneumatic platform depicted in Fig. 3, which is used to control the air pressure in the actuator and to acquire data signals. The air chamber of the actuator

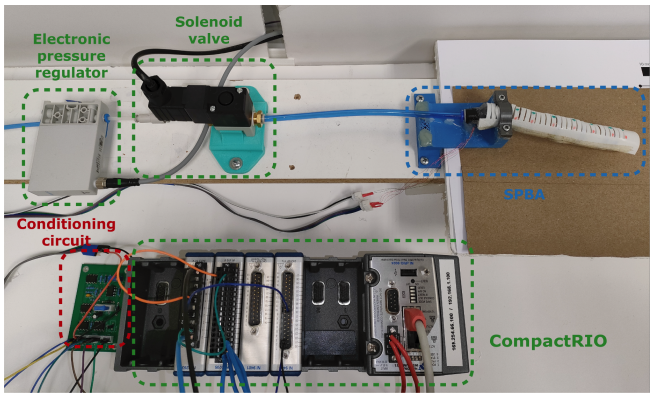

Fig. 4. Experimental setup of the SPBA.

is pneumatically connected to an electronic pressure regulator (Festo™ VEAB-L-26-D7-Q4-V1-1R1) and a solenoid valve (SMC© EVT307-6DO-02F-Q), shown in Fig. 4. The conditioning circuit from [19] is used to adapt the resistive signal of the actuator through the measuring electrodes depicted in Fig. 1, following the *four-probe method*. The National Instruments™ CompactRIO 9024 is responsible for acquiring the actuator curvature signal after the conditioning circuit. This curvature signal is calibrated using a curve detection algorithm on the images obtained by a camera positioned above the actuator. In addition, the curvature data obtained by the algorithm serve as ground truth during the experiments. The CompactRIO is also used for implementing the FOC and commanding the pressure regulator and the solenoid valve.

The dynamics of the electronic pressure regulator was identified in [20] as a second order transfer function:

$$R(s) = \frac{152.48}{s^2 + 53.39 \cdot s + 1528} \tag{1}$$

The measurements obtained with the conditioning circuit have been filtered to reduce the high frequency noise with a lowpass filter of the form:

$$H(s) = \frac{10}{s + 10} \tag{2}$$

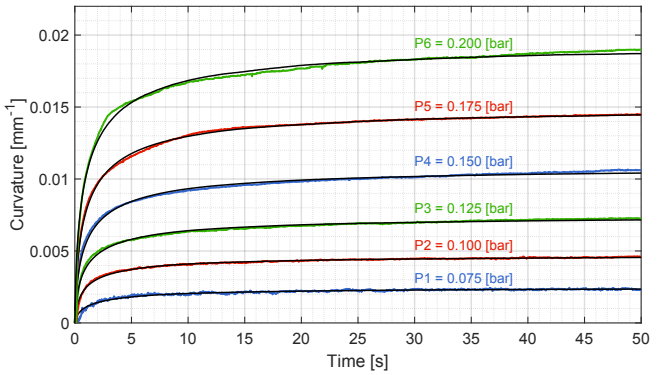

Fig. 5. Curvature evolution of the SPBA to different pressure steps (colored plots) using a computer vision algorithm. Black lines represent the curvature evolution simulated with the identified FOMs.

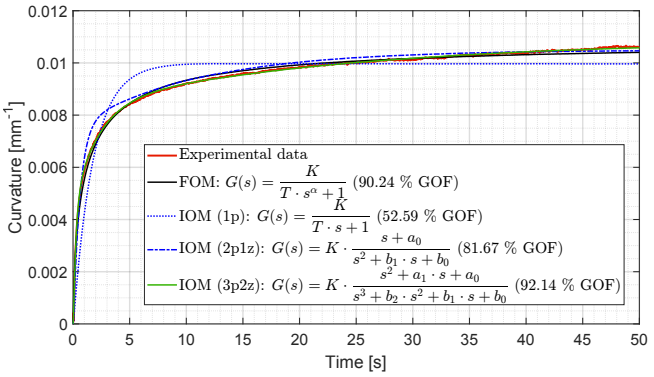

Fig. 6. Different models fitting the SPBA response to an input pressure step of 0.15 bar. Intermediate IOM between those represented have been omitted since their responses are not significantly different. The labels p and z indicate the number of poles and zeros.

Both dynamics will be taken into account in Section IV in the controller design.

III. FRACTIONAL ORDER EXPERIMENTAL MODELING

In this Section, an experimental procedure for tuning the FOM parameters of SPBAs is presented. This procedure uses step inputs with regularly-spaced amplitudes within the range of the control signal to obtain a set of responses that can be used in the fitting process.

In the specific case of our unidirectional SPBA, it was excited along a wide operating range, varying input pressure steps from 0.075 to 0.2 bar in steps of 0.025 bar. The time evolution of the curvature to these step inputs is shown in Fig. 5, where the nonlinear behavior of the SPBA is obvious from the variable increasing change in the steady-state values of the curvature. This undesired behavior is a consequence of the viscoelasticity and hyperelasticity of the CN-Hydrogel.

As these responses show an overdamped behavior of the system, it is determined that the simplest FOM that can represent this type of behavior has the form:

$$G(s) = \frac{K}{T \cdot s^{\alpha} + 1} \tag{3}$$

where K is the gain of the model, T is a constant related to the rise time and α is the fractional order of the model, which ranges from 0 (simple gain with no dynamics) to 1 (classical first order IOM system).

The parameters of this FOM have been adjusted with the Levenberg-Marquardt least-squares algorithm using the `pfid` function of the MATLAB Fractional Modeling and Control Toolbox, FOMCON[1]. In addition, to demonstrate the advantages of using a FOM, different IOMs have also been fitted with the same algorithm, using the MATLAB `ftest` function.

For comparison purposes, the simulated responses of each one of these models to an input pressure step of 0.15 bar, are shown in Fig. 6. It is observed that the fractional model follows closely the response of the experimental data, with a goodness of fit (GOF) over 90%. This GOF is defined as a normalized root mean squared error with the form:

$$GOF = 1 - \frac{\|y_{exp} - y_{sim}\|}{\|y_{exp} - \bar{y}_{exp}\|} \tag{4}$$

where y_{exp} is the data of the experiment to fit, $\bar{y}_{exp}$ the mean of the same experiment, y_{sim} the simulated response of the fitted model, and $\|\cdot\|$ represents the euclidian norm.

TABLE I
GOFs OF THE FITTED MODELS UNDER THE PRESSURE STEPS

Input Press. (bar)	FOM	IOM (1p)	IOM (2p1z)	IOM (3p2z)
0.075	0.7594	0.5954	0.7239	0.7668
0.100	0.8791	0.5880	0.8201	0.8818
0.125	0.8805	0.5180	0.8286	0.9058
0.150	0.9024	0.5259	0.8167	0.9214
0.175	0.9212	0.5806	0.8309	0.9103
0.200	0.9062	0.5695	0.8358	0.9294
Mean results	0.8748	0.5629	0.8093	0.8859

Table I reports the GOFs obtained after fitting the models proposed in Fig. 6 to all the pressure steps. It can be seen that to obtain an average response with equal or better GOF than the FOM, it is necessary to resort to an IOM of higher order (at least with 3 poles and 2 zeros). Associated with complexity, the higher order IOM suffers from having more parameters to adjust, which mainly leads to more complicated controllers. Hence, the calculated FOM is deemed the best choice among the models examined.

The parameters K, T and α of the chosen model are tuned separately for the response to each different input pressure reference, obtaining the black lines shown in Fig. 5. The values of the parameters versus the input pressure are plotted in Fig. 7, where we observe that both T and α can be approximated as constants, while K perfectly adjusts ($R^2 = 0.9989$) to a straight line, most likely due to the hyperelasticity of the material, as higher pressures cause much higher deformation.

Hence, the final adjusted FOM is as follows:

$$G(s) = \frac{K(p)}{1.32 \cdot s^{0.6} + 1} \tag{5}$$

[1]Available at `https://fomcon.net/`

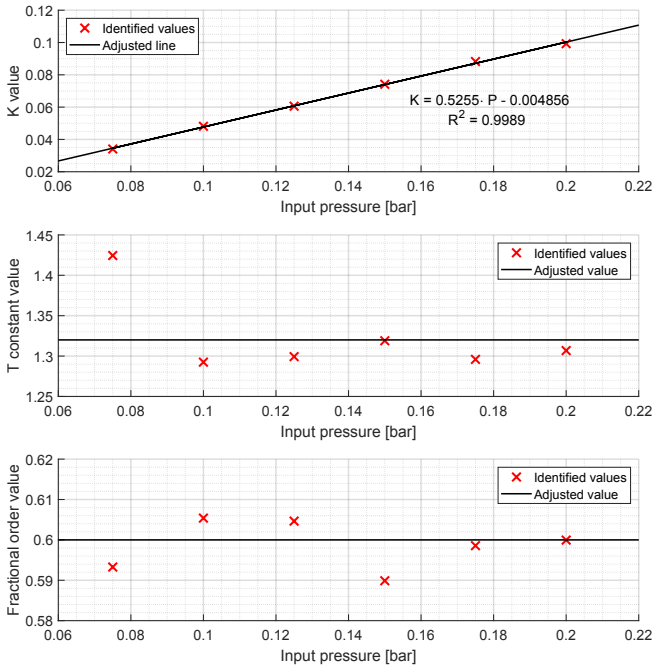

Fig. 7. Adjusted parameters of the proposed FOM at each pressure step. The K value is shown in the upper graph, the T term in the middle one and the fractional order α of the model is shown in the lower plot.

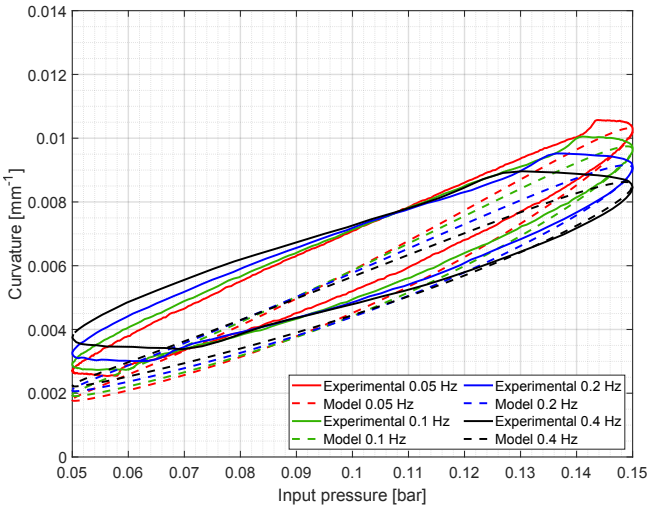

Fig. 8. Curvature described by the SPBA under different sinusoidal input pressures with an amplitude of 0.05 bar and an offset of 0.1 bar (solid lines) and the curvature described by the FOM under the same input pressures (dashed lines). Note that these curves represent stable cycles, ignoring the initial transient ones.

where $K(p)$ is a variable parameter that depends on the input pressure p, according to the line equation shown in Fig. 7. In a way, this parameter models the hyperelasticity of the actuator.

Limitations of the adjusted model

Fig. 8 shows the curvature described by the SPBA when it is excited with a sinusoidal pressure signal of amplitude 0.05 bar, with an offset of 0.1 bar. To get a better idea of how frequency affects the SPBA, this sine signal has been particularized at four different low frequencies: 0.05 Hz, 0.1 Hz, 0.2 Hz and 0.4 Hz. This figure shows how the actuator describes different trajectories when periodically pressurized and depressurized, presenting hysteresis, which is a characteristic of pneumatically actuated systems.

In addition, it can be observed how the frequency affects the curvature extremes reached, decreasing its maximum and increasing its minimum as the frequency increases, as a consequence of the loss of magnitude of the system in the frequency range studied.

The input pressure generated for the SPBA (recorded with the CompactRIO at the output of the pressure regulator) is used as input for the model described by (5), obtaining the results plotted with the dashed lines in Fig. 8. It can be seen that the model does not accurately capture the response of the SPBA under a sinusoidal signal, specially during depressurization.

The main reason for this difference is that the model has been fitted uniquely with positive steps, representing the behaviour of the SPBA during the air compression. The dynamics of the actuator and the pneumatic system in the event of decompression will be different due to viscoelasticity, hyperelasticity and pneumatic actuation.

The model, however, matches the experimental data at the highest pressure input (right end of each curve), validating the adjustment of the FOM for positive steps.

IV. FRACTIONAL ORDER CONTROL

This Section proposes the design of FOC controllers for SPBAs based on the inversion of the FOM model.

First of all, it is necessary to study which terms (poles and zeros) of the system prevent the desired behaviour. These terms should be cancelled during the model inversion. Our FOM has a single pole, responsible for all the dynamics. Therefore, cancelling this pole with its corresponding zero will speed up the response of the SPBA. This zero is implemented in our control system using the algorithm described in the Appendix, based on the Grünwald-Letnikov definition with the short memory principle [21].

The implemented controller also compensates the gain $K(p)$ of the model, requiring the adjustment of the gain of the controller K_o. To ensure zero steady-state error of the feedback system, an integer order integrator $1/s$ is cascaded with the controller. This term is implemented using a trapezoidal integrator, so no error would arise due to the limited memory of the Grünwald-Letnikov implementation. Thus, the designed FOC is:

$$C(s) = \frac{K_o(p)}{K(p)} \cdot (1.32 \cdot s^{0.6} + 1) \cdot \frac{1}{s} \tag{6}$$

where K_o has been adjusted as a pressure dependent variable gain to adapt the controller to the changes of $K(p)$. This $K_o(p)$ has been determined, by studying the complete system in simulation, and validated experimentally as:

$$K_o(p) = 85.66 \cdot p + 6.692 \tag{7}$$

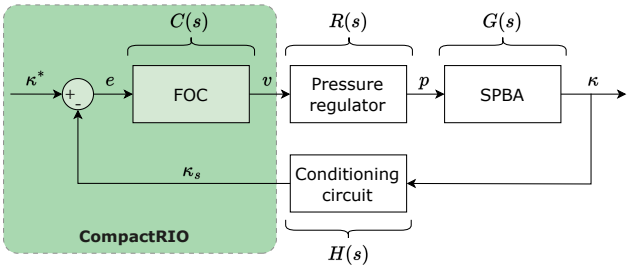

Fig. 9. Closed loop control scheme for the SPBA's curvature.

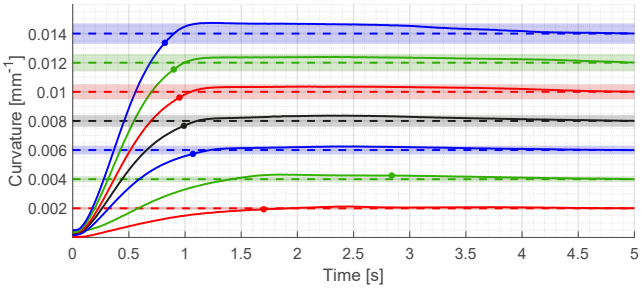

(a) Time responses of the SPBA curvature obtained with the proprioceptive sensor (not the vision algorithm). For each signal, the reference is shown with the dashed line, the $\pm 5\%$ band with the shaded region and the settling time with a round marker.

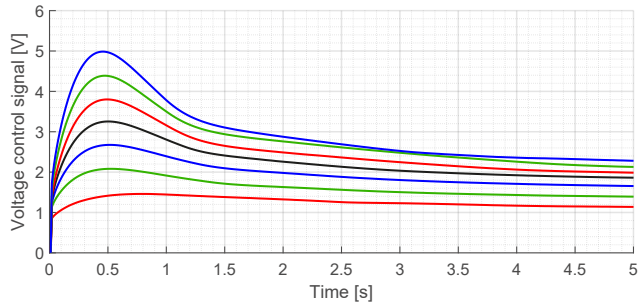

(b) Voltage control signals.

Fig. 10. Curvature of the SPBA and control signals under different curvature step setpoints.

The simplest feedback control scheme resulting from applying this FOC controller in our platform is presented in Fig. 9. The time responses obtained with this controller can be seen in Fig. 10, where 7 consecutive different curvature setpoints have been tested. Notice how the initial curvature of the SPBA starts on a different point between experiments. This is due to the displacement of the relaxation stress caused by the viscoelasticity of the material. The tested curvature setpoints start at 0 mm^{-1} and range from 0.002 mm^{-1} to 0.014 mm^{-1} (see Fig. 11), covering a wide range of operation. The average settling time is 1.5 seconds for a tolerance band of 5% with an overshoot of less than 5% from the third signal onwards, validating the designed FOC.

Regarding the control signal, the difference between its steady-states decreases as the curvature setpoint increases, pointing out the softening that the material undergoes as a consequence of hyperelasticity.

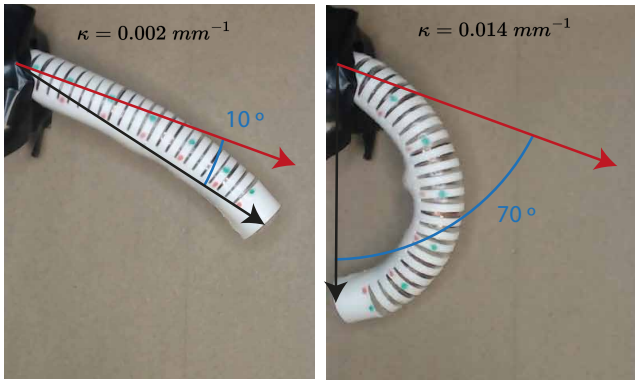

Fig. 11. Unidirectional SPBA. Figure left and right show the actuator at two different curvatures and their reached angle.

V. CONCLUSIONS

This article seeks to demonstrate how fractional order models and controllers can be applied to simplify the complicated nonlinear dynamics of SPBAs.

First, we present our SPBA, describing its design and fabrication. For this work, we take advantage of the *self-sensing* property of our hydrogel, which allows the controllability of the SPBA.

Then, we present an experimental procedure for the easy calculation of FOMs for SPBAs. As a main contribution in this work, we demonstrate how an empirical FOM with a low number of parameters performs equally well as high order integer models with many more terms. However, it is important to acknowledge that these empirically obtained FOMs still neglect significant dynamics, particularly the hysteresis. This is mainly because, in this work, we have focused on positive pressure movements. For a comprehensive characterization of the hysteresis of SPBA, both positive and negative movements must be studied. Nevertheless, our main motivation lies in the simplicity of the model, which enables easy implementation (e.g., through model inversion) of fractional order controllers. Indeed, we present a simple procedure for obtaining FOCs for our SPBA by inverting the FOM, what is possible due to its simplicity.

APPENDIX

IMPLEMENTATION OF FRACTIONAL ORDER TRANSFER FUNCTIONS

In this appendix, we present the numerical algorithm used to implement fractional order transfer functions in this work. This algorithm has been derivated from the one presented in [22].

A continuous fractional order transfer function is defined as:

$$G(s) = \frac{\sum_{i=0}^{m} b_i s^{\beta_i}}{\sum_{i=0}^{n} a_i s^{\alpha_i}} \tag{8}$$

This transfer function represents the relationship between an input $u(t)$ and an output $y(t)$ of a fractional order differential equation of the form:

$$\sum_{i=0}^{n} a_i \mathscr{D}^{\alpha_i} y(t) = \sum_{i=0}^{m} b_i \mathscr{D}^{\beta_i} u(t) \tag{9}$$

Making use of the Grünwald-Letnikov definition for the fractional order derivative $\mathscr{D}^{\alpha} f(t)$ with the short memory principle [21] and zero initial conditions, one can obtain, after discretization ($t_k = kh$, $y_k = y(t_k)$ and $u_k = u(t_k)$, where h is the step size), the expression:

$$y_k = \frac{u_k \cdot \sum_{i=0}^{m} B_i + \left(\sum_{i=0}^{m} B_i \cdot \sum_{j=1}^{L} w_{j,i+n+1} \cdot u_{k-j} \right)}{\sum_{i=0}^{n} A_i} - \frac{\left(\sum_{i=0}^{n} A_i \cdot \sum_{j=1}^{L} w_{j,i} \cdot y_{k-j} \right)}{\sum_{i=0}^{n} A_i} \tag{10}$$

where $w_{j,i}$ represents, in a matrix form, the binomial coefficients calculated recursively with the equations:

$$w_{0,i} = 1, \qquad w_{j,i} = w_{j-1,i} \cdot \left(1 - \frac{\alpha_i + 1}{j} \right) \tag{11}$$

for $i = 0, 1, \cdots, n$. And:

$$w_{0,i+n+1} = 1, \; w_{j,i+n+1} = w_{j-1,i+n+1} \cdot \left(1 - \frac{\beta_i + 1}{j} \right) \tag{12}$$

for $i = 0, 1, \cdots, m$, both with $j = 1, 2, \cdots, L$, where L is the memory length used for the short memory principle. Furthermore, A and B are the terms that contains the coefficients of the derivatives, defined as:

$$A_i = a_i \cdot h^{-\alpha_i}, \qquad i = 0, 1, \cdots, n \tag{13}$$

$$B_i = b_i \cdot h^{-\beta_i}, \qquad i = 0, 1, \cdots, m \tag{14}$$

Hence, expressions (10) to (14) are used for the discrete implementation of fractional order transfer functions. Within the scope of this work, these equations have been used for the FOC implementation, (6), in the CompactRIO controller, using the LabVIEW Real-Time SCAN Engine.

REFERENCES

[1] H. K. Yap, J. H. Lim, F. Nasrallah, J. C. Goh, and R. C. Yeow, "A soft exoskeleton for hand assistive and rehabilitation application using pneumatic actuators with variable stiffness," in *2015 IEEE international conference on robotics and automation (ICRA)*. IEEE, 2015, pp. 4967–4972.

[2] S. Abondance, C. B. Teeple, and R. J. Wood, "A dexterous soft robotic hand for delicate in-hand manipulation," *IEEE Robotics and Automation Letters*, vol. 5, no. 4, pp. 5502–5509, 2020.

[3] S. Terryn, J. Langenbach, E. Roels, J. Brancart, C. Bakkali-Hassani, Q.-A. Poutrel, A. Georgopoulou, T. G. Thuruthel, A. Safaei, P. Ferrentino *et al.*, "A review on self-healing polymers for soft robotics," *Materials Today*, vol. 47, pp. 187–205, 2021.

[4] J. Wang and A. Chortos, "Control strategies for soft robot systems," *Advanced Intelligent Systems*, vol. 4, no. 5, p. 2100165, 2022.

[5] M. S. Xavier, C. D. Tawk, A. Zolfagharian, J. Pinskier, D. Howard, T. Young, J. Lai, S. M. Harrison, Y. K. Yong, M. Bodaghi *et al.*, "Soft pneumatic actuators: A review of design, fabrication, modeling, sensing, control and applications," *IEEE Access*, vol. 10, pp. 59 442–59 485, 2022.

[6] V. Falkenhahn, T. Mahl, A. Hildebrandt, R. Neumann, and O. Sawodny, "Dynamic modeling of bellows-actuated continuum robots using the euler–lagrange formalism," *IEEE Transactions on Robotics*, vol. 31, no. 6, pp. 1483–1496, 2015.

[7] P. Polygerinos, Z. Wang, J. T. B. Overvelde, K. C. Galloway, R. J. Wood, K. Bertoldi, and C. J. Walsh, "Modeling of soft fiber-reinforced bending actuators," *IEEE Transactions on Robotics*, vol. 31, no. 3, pp. 778–789, 2015.

[8] L. Gharavi, M. Zareinejad, and A. Ohadi, "Dynamic finite-element analysis of a soft bending actuator," *Mechatronics*, vol. 81, p. 102690, 2022.

[9] W. Chen, C. Xiong, C. Liu, P. Li, and Y. Chen, "Fabrication and dynamic modeling of bidirectional bending soft actuator integrated with optical waveguide curvature sensor," *Soft robotics*, vol. 6, no. 4, pp. 495–506, 2019.

[10] K. Bingi, B. Rajanarayan Prusty, and A. Pal Singh, "A review on fractional-order modelling and control of robotic manipulators," *Fractal and Fractional*, vol. 7, no. 1, p. 77, 2023.

[11] M. K. Mishra, A. K. Samantaray, and G. Chakraborty, "Fractional-order Bouc-Wen hysteresis model for pneumatically actuated continuum manipulator," *Mechanism and Machine theory*, vol. 173, p. 104841, 2022.

[12] H. Shi, Y. Liu, P. Chen, Y. Luo, and Y. Chen, "Fractional-order dynamics modeling for continuum robots," in *2023 International Conference on Fractional Differentiation and Its Applications (ICFDA)*. IEEE, 2023, pp. 1–5.

[13] M. Luo, E. H. Skorina, W. Tao, F. Chen, S. Ozel, Y. Sun, and C. D. Onal, "Toward modular soft robotics: Proprioceptive curvature sensing and sliding-mode control of soft bidirectional bending modules," *Soft robotics*, vol. 4, no. 2, pp. 117–125, 2017.

[14] C. A. Monje, F. Ramos, V. Feliu, and B. M. Vinagre, "Tip position control of a lightweight flexible manipulator using a fractional order controller," *IET Control Theory & Applications*, vol. 1, pp. 1451–1460, September 2007. [Online]. Available: https://digital-library.theiet.org/content/journals/10.1049/iet-cta_20060477

[15] C. A. Monje, B. Deutschmann, J. Muñoz, C. Ott, and C. Balaguer, "Fractional order control of continuum soft robots: Combining decoupled/reduced-dynamics models and robust fractional order controllers for complex soft robot motions," *IEEE Control Systems Magazine*, vol. 43, no. 3, pp. 66–99, 2023.

[16] J. de la Morena, A. López-Díaz, F. Ramos, I. Payo, and A. S. Vázquez, "Modular bending actuators based on self-x properties of the CN-Hydrogel," in *2024 IEEE 7th International Conference on Soft Robotics (RoboSoft)*, p. Accepted.

[17] A. Naranjo, C. Martín, A. López-Díaz, A. Martín-Pacheco, A. M. Rodríguez, F. J. Patiño, M. A. Herrero, A. S. Vázquez, and E. Vázquez, "Autonomous self-healing hydrogel with anti-drying properties and applications in soft robotics," *Applied Materials Today*, vol. 21, p. 100806, dec 2020.

[18] A. López-Díaz, J. De La Morena, F. Ramos, E. Vázquez, and A. S. Vázquez, "A novel hydrogel-based connection mechanism for soft modular robots," in *2022 International Conference on Robotics and Automation (ICRA)*. IEEE, 2022, pp. 7124–7130.

[19] A. López-Díaz, A. Braic, F. Ramos, I. Payo, E. Vázquez, and A. S. Vázquez, "Hydrogel-based soft pneumatic bending actuator with self-healing and proprioception capabilities," in *2022 IEEE 5th International Conference on Soft Robotics (RoboSoft)*. IEEE, 2022, pp. 370–375.

[20] A. López-Díaz, J. de la Morena, A. Braic, C. Serna, F. Ramos, E. Vázquez, and A. S. Vázquez, "Proprioception and control of a soft pneumatic actuator made of a self-healable hydrogel," *Soft robotics*, p. Accepted, 2024.

[21] I. Podlubny, "Numerical solution of ordinary fractional differential equations by the fractional difference method," *Advances in Difference Equations*, 1997.

[22] C. A. Monje, Y. Chen, B. M. Vinagre, D. Xue, and V. Feliu, *Fractional-order Systems and Controls*. Springer London, 2010.